P H Y S I C A L   R E V I E W   L E T T E R S

Nonlinear Wavelength Selection in Surface Faceting under Electromigration

Fatima Barakat, Kirsten Martens, and Olivier Pierre-Louis

Laboratoire de Physique de la Matière Condensée et Nanostructures, Université Lyon 1,
43 Bd du 11 novembre, 69622 Villeurbane, France
(Received 26 March 2012; published 31 July 2012)

We report on the control of the faceting of crystal surfaces by means of surface electromigration. When electromigration reinforces the faceting instability, we find perpetual coarsening with a wavelength increasing as $t^{1/2}$. For strongly stabilizing electromigration, the surface is stable. For weakly stabilizing electromigration, a cellular pattern is obtained, with a nonlinearly selected wavelength. The selection mechanism is not caused by an instability of steady states, as suggested by previous works in the literature. Instead, the dynamics is found to exhibit coarsening *before* reaching a continuous family of stable nonequilibrium steady states.

In nonequilibrium conditions, crystal surfaces undergo various instabilities leading to micro- or nanostructures. The ultimate faith of these topographical structures is governed by the nonlinear dynamics of the surface. Understanding the nonlinear processes at play is therefore important for many applications where one wishes to design structures with a given wavelength. However, the complexity of nonlinear wavelength selection mechanisms have hindered their control, and strategies to achieve predictive design are still poorly understood. A possible strategy is to control existing instabilities by means of an external field. Here we explore the control of the faceting instability with electromigration. The faceting instability is the decomposition of a surface with a given average orientation into neighboring facetted orientations [1–6]. This instability is of thermodynamic origin, and is driven by the reduction of the surface free energy. The presence of an electric current leads to a surface electromigration mass flux J_E. This mass flux can stabilize or destabilize crystalline surfaces depending on its orientation-dependence [7–13]. Many studies have been devoted to these two instabilities. The combination of electromigration and anisotropy is already known to lead to nontrivial dynamics of voids, with the appearance of nontrivial orientations and oscillatory dynamics [14]. In this Letter, we show that a faceting instability can be controlled by electromigration. In the presence of destabilizing electromigration, the faceting instability is found to be reinforced, and perpetual coarsening with a wavelength increasing as $t^{1/2}$ is found. Strongly stabilizing electromigration supersedes the faceting instability and stabilizes the surface. This result is similar to the stabilization of the elastic stress-induced Grinfeld instability by electromigration discussed in Ref. [15]. Our most striking result appears in the presence of weakly stabilizing electromigration: when starting from random initial conditions, a wavelength larger than that emerging from the linear instability is selected. Usual nonlinear wavelength selection scenarios emerge from an instability of periodic steady states. Examples of these scenarios include interrupted coarsening [16–18] and secondary instabilities such as the Eckhaus instability [19]. Our scenario is different: we find a stable steady state branch, and coarsening occurs before the system reaches any steady state.

Model.—Combining previous works on faceting [4,5] and on electromigration-induced instabilities [11–13], we write down a phenomenological nonlinear equation which governs surface dynamics. We use a one-dimensional model for the crystal surface height profile $h(x, t)$ and slope $\phi(x, t) = \partial_x h(x, t)$. The average orientation $\phi = 0$ of the surface is assumed to be unstable, and to decompose into facets of slopes $\phi = \pm 1$. For the sake of simplicity, we consider a Ginzburg-Landau-like orientation dependent energy:

$$\mathcal{F}[\phi] = \gamma \int dx \left[-\frac{\phi^2}{2} + \frac{\phi^4}{4} + \frac{\epsilon^2}{2}(\partial_x \phi)^2 \right], \quad (1)$$

where γ is a typical surface energy scale. The last term on the r.h.s. accounts for a curvature energy cost, which regularizes facets [4,5] at the cutoff length ϵ. This length scale could, e.g., account for the distance between atomic steps running on the facet. From Eq. (1), the local chemical potential is derived as

$$\mu = \Omega \frac{\delta \mathcal{F}[\phi]}{\delta h} = \gamma \Omega \partial_x [\epsilon^2 \partial_{xx} \phi + \phi - \phi^3]. \quad (2)$$

where Ω is the atomic area. We consider surface-diffusion limited dynamics, so that chemical potential gradients induce a surface mass flux $J_\mu = -D_L \partial_x \mu / k_B T$, where $k_B T$ is the thermal energy. In addition, we assume that an external electric current is applied to the crystal, leading to an orientation-dependent electromigration surface mass flux $J_E(\phi)$. Expanding the electromigration current for small slopes, we write $J_E(\phi) \approx J_E(0) + \phi J'_E(0)$. The slope-dependence of J_E may either be caused by the anisotropy of surface diffusion [11,20] or migration

force [21]. As shown in Fig. 1(a), electromigration is destabilizing when $J_E'(0) > 0$, and stabilizing when $J_E'(0) < 0$. This instability is the subject of a large literature, and has been the basis of the interpretation of the instabilities observed on semiconductors [7] and on metals [22]. Mass conservation reads $\partial_t h = -\Omega \partial_x [J_\mu + J_E]$, and leads to an evolution equation for the surface height:

$$\frac{\partial_t h}{\Omega} = D_L \frac{\Omega \gamma}{k_B T} \partial_{xx}[\epsilon^2 \partial_{xxxx} h + \partial_{xx} h - \partial_x(\partial_x h)^3]$$
$$- J_E'(0)\partial_{xx} h, \tag{3}$$

where we have assumed for simplicity that D_L does not depend on the orientation. Clearly, additional nonlinear terms could enter into play, such as higher order terms in the expansion of J_E, or an orientation dependence of D_L in J_μ. However, since it is the simplest model which accounts for the combined action of faceting and electromigration, we shall focus on Eq. (3) in the following. Normalizing x with ϵ, t with $k_B T \epsilon^4 / \Omega^2 \gamma D_L$, and defining the dimensionless parameter $j_E' = J_E'(0) k_B T \epsilon^2 / \Omega \gamma D_L$, we may write a one-parameter equation for the slope:

$$\partial_t \phi = \partial_{xxxx}[\partial_{xx}\phi + \phi - \phi^3] - j_E' \partial_{xx}\phi. \tag{4}$$

The relaxation part of Eq. (4), first derived in Ref. [5], is expected to give rise to perpetual logarithmic coarsening [23]. The electromigration part has been derived and used in many papers, see Ref. [13] for a review. Electromigration without faceting is expected to lead to power-law coarsening [13]. Here, we claim that the combination of the two physical processes—faceting and electromigration—gives rise to novel dynamics.
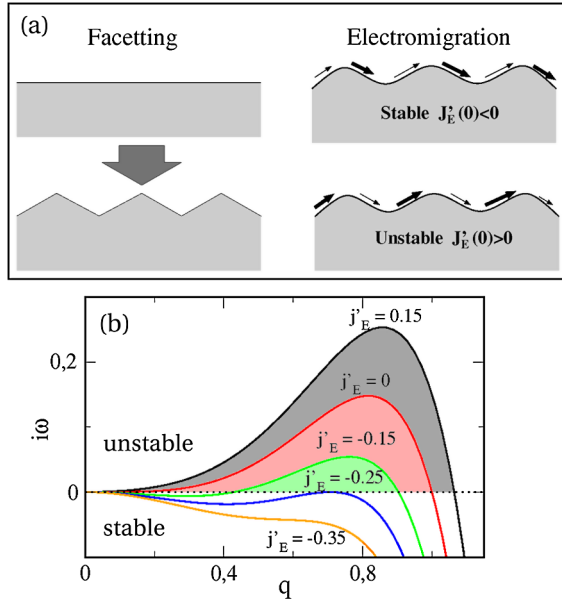

FIG. 1 (color online). *Mechanism of the instability and dispersion relation*—(a) Schematics of the faceting and electromigration-induced instabilities. (b) Growth rate $i\omega$ of Fourier modes from linear stability analysis, see Eq. (5).

Linear stability analysis.—Let us start the study of Eq. (4) by means of a linear stability analysis. The growth rate $i\omega$ of a Fourier mode $\sim e^{i\omega t + iqx}$ of wavelength $\lambda = 2\pi/q$ reads:

$$i\omega = -q^6 + q^4 + j_E' q^2. \tag{5}$$

As shown on Fig. 1, we obtain three regimes. (i) For $j_E' \gtrsim 0$, all wavelengths larger than $\lambda_- = 2\pi/[1/2 + (1/4 + j_E')^{1/2}]^{1/2}$ are unstable. (ii) When electromigration is weakly stabilizing $0 > j_E' > -1/4$, there is a finite range of unstable wavelengths $\lambda_- < \lambda < \lambda_+$ where $\lambda_+ = 2\pi/[1/2 - (1/4 + j_E')^{1/2}]^{1/2}$. (iii) Finally, for strongly stabilizing electromigration, when $j_E' < -1/4$, the surface is linearly stable. When the surface is unstable, the wavelength $\lambda_m = 2\pi 3^{1/2}/[1 + (1 + 3j_E')^{1/2}]^{1/2}$ of the fastest growing mode is expected to emerge from random initial conditions (where all modes are present).

As an example, we consider Si(111) vicinal surfaces where both electromigration-induced instabilities [7–10] and faceting have been observed. Faceting on Si(111) vicinal surfaces could be induced by surface energies, as in Refs. [24,25], or by small coverage of metal atoms, as observed in several experiments [26,27]. Assuming attachment-detachment-limited step dynamics following Ref. [28], one has $J_E'(0)/\gamma D_L \approx -F/\phi k_B T$, where F is the electromigration force. The typical distance between atomic steps is $d \sim 10^2$–10^3 Å. Assuming $\epsilon \sim d$ and using $|F|/k_B T \sim 10^8$ Å, and $\gamma \sim 0.1$ eV Å^{-2}, we find $|j_E'| \sim 10^{-2} - 10$, suggesting that the three stability regimes could be observed in experiments. In addition, experimental observations could provide quantitative informations on the phenomenological cutoff length ϵ, that enters in many macroscopic models with facets [4,5,23,29,30].

Lyapunov functional.—The linear stability analysis predicts the existence or not of an instability from small initial perturbations. However, the amplitude of the unstable modes increases exponentially fast, and the unstable front enters into the nonlinear regime where the ϕ^3 term in Eq. (4) is not negligible anymore. While the analytical study of the nonlinear regime is in general delicate, the presence of a Lyapunov function $\mathcal{L}$, i.e., a quantity which monotonically decreases during the dynamics, greatly simplifies the analysis. Here, we define

$$\mathcal{L}[h] = \mathcal{F}[\partial_x h] - \frac{j_E'}{2}\int dx h(x)^2. \tag{6}$$

Indeed, one may write $\partial_t h = \partial_{xx}[\delta\mathcal{L}/\delta h]$, leading to:

$$\partial_t \mathcal{L} = -\int dx [\partial_x(\delta\mathcal{L}/\delta h)]^2 \leq 0. \tag{7}$$

Steady state branches.—The space of all possible configurations for the surface profile is very large, and it is impossible to evaluate $\mathcal{L}$ for all configurations. As a consequence, we would like to reduce this space to a relevant subset of shapes which is simpler to explore.

A powerful approach along this line is to study the steady states $\phi_0(x)$, which are the solutions of $\partial_t\phi_0 = 0$. Using Eq. (7), one has $\partial_x(\delta\mathcal{L}/\delta h) = 0$, leading to

$$\partial_{xx}[\partial_{xx}\phi_0 + \phi_0 - \phi_0^3] - j_E'\phi_0 = 0. \quad (8)$$

The central idea motivating the study of steady states is the existence of a separation of time scales, where the shape first relaxes rapidly toward periodic steady states. Then, these periodic solutions may exhibit an instability occurring at longer time scales, leading for example to a coarsening process [18], or to the Eckhaus instability [19].

The steady states profiles are obtained numerically, starting with a small amplitude sinusoidal perturbation $\sim \sin(2\pi x/\lambda)$ with one period in a box of width λ [31]. Following the linear stability analysis, the perturbation may grow or decay. When it grows, it reaches a finite amplitude steady state where it stops. As shown in Fig. 2(a) for $j_E' > 0$, the steady state exhibits a monotonically increasing amplitude A as a function of the wavelength λ. Asymptotically for large A and λ, we expect the dominant term among the linear terms to be the one with the fewest derivatives, i.e. $j_E'\phi_0$, and this term has to balance the nonlinear term $\partial_{xx}\phi_0^3$, leading to $A \sim (j_E')^{1/2}\lambda$. The numerical determination of the steady-state branch actually indicates that $A \approx 0.16(j_E')^{1/2}\lambda$ for $\lambda \gg \lambda_-$.

When $-1/4 < j_E' < 0$, we obtain a bell shape branch connecting the two marginal points ($\lambda = \lambda_-$, $A = 0$), and ($\lambda = \lambda_+$, $A = 0$), as shown in Fig. 3(a). In addition, using suitable initial conditions, we find another steady-state branch, which emerges from the primary bell-shape branch. The typical steady-state profiles are shown on Fig. 3(d). Other branches could exist, and we have not tried to provide a complete analysis of all possible
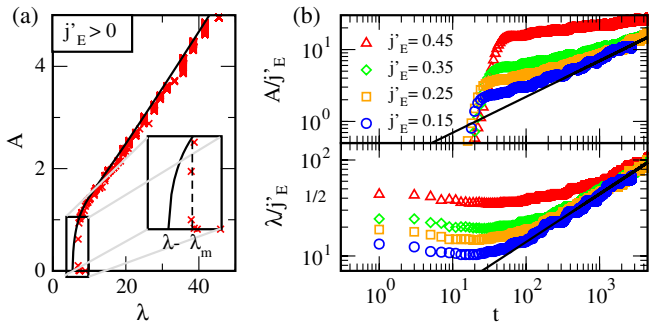
steady-state branches. However, and as discussed in the following, the study of the main bell-shape branch seems to be sufficient to account for the main features of the full dynamics starting from small random perturbations.

The numerical calculation of $\mathcal{L}$ along the steady-state branches shows that $\mathcal{L}$ decreases monotonically with λ for $j_E' > 0$, while it exhibits a minimum for $\lambda = \lambda_{\mathcal{L}}$ when $-1/4 < j_E' < 0$. At this point, it is tempting to speculate that the dynamics will simply follow the gradient of $\mathcal{L}$ along the steady-state branches leading to infinite coarsening when $j_E' > 0$ and interrupted coarsening at $\lambda = \lambda_{\mathcal{L}}$ for $-1/4 < j_E' < 0$. We shall see in the following that some of these speculations are actually wrong.

Steady-state stability.—In order to analyze the dynamics more carefully, we shall investigate the stability of steady states with respect to small perturbations $\phi_1(x) = \phi(x) - \phi_0(x) \ll \phi_0(x)$. The slope variation ϕ_1, leads to the following variation of $\mathcal{L}$:

$$\mathcal{L}_1 = \frac{1}{2}\int dx[\phi_1^2(3\phi_0^2 - 1) + (\partial_x\phi_1)^2 - j_E'h_1^2], \quad (9)$$

where $\partial_x h_1 = \phi_1$. Physically relevant steady states must be stable with respect to perturbations with wavelengths
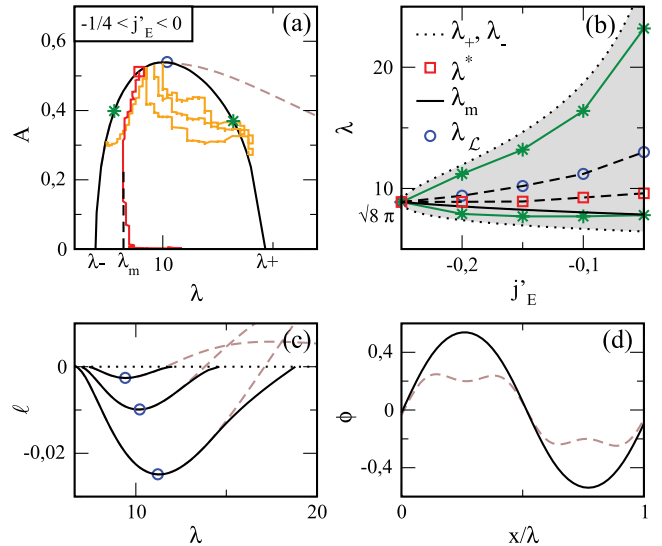

FIG. 2 (color online). *Perpetual power-law coarsening for* $j_E' > 0$—(a) The black line indicates the steady-state amplitude A versus wavelength λ of periodic steady states for $j_E' = 0.45$ extracted from the profiles of periodic steady states. Crosses ($\times$): full simulations of Eq. (4) from small random initial conditions in a large system of size $L = 500$, as in Fig. 4(a). (b) Rescaled Amplitude A/j_E' and wavelength $\lambda/(j_E')^{1/2}$ as function of time in a large system starting from small random initial conditions. The solid lines are the power laws discussed in the text.

FIG. 3 (color online). *Nonlinear wavelength selection for* $-1/4 < j_E' < 0$—(a) The (black) solid and (brown) dashed lines indicate the steady-state amplitude A versus wavelength λ for $j_E' = -0.15$. Red line: full simulations of Eq. (4) from small random initial conditions in a large system of size $L = 500$, as in Fig. 4(b). Orange lines: dynamics starting from slightly perturbed periodic steady state in an extended system. Green stars indicate theoretical limit of stability of the steady-state branch. (b) The shaded region corresponds to the linearly unstable region. Green stars: limits of steady-state stability. (c) Lyapunov functional density $\ell = \mathcal{L}/L$ where L is the system size, evaluated from the steady-state profiles. (d) Steady-state profiles numerically obtained for the two branches at $j_E' = -0.15$.

smaller than their periodicity, and in general, we expect that the most dangerous modes are long-wavelength perturbations, as pointed out, e.g., in Ref. [18]. In the long wavelength limit, where the perturbation wavelength is much larger than the periodicity of the steady state ϕ_0, one may simply replace $\phi_0^2(x)$ by its average over one period $\langle \phi_0^2 \rangle$. Thus, since it has constant coefficients, Eq. (9) is now diagonal in Fourier space, and this suggests a simple stability criterion:

$$(3\langle \phi_0^2 \rangle - 1)q_1^2 + q_1^4 - j_E' > 0. \tag{10}$$

As a consequence, long wavelength modes $q_1 \to 0$ are always unstable in the case of destabilizing electromigration $j_E' > 0$. This is in agreement with the above speculation of perpetual coarsening. In addition, we may also gain information about the coarsening exponent. Indeed, at long wavelengths we have $\mathcal{L}_1 \approx -\int dx j_E' h_1^2/2$, and as a consequence one has $\partial_t h_1 \approx -j_E' \partial_{xx} h_1$. This relation provides a link between lengthscales x, assumed to be $\sim \lambda$, and time scales t, leading to $\lambda \sim (j_E')^{1/2} t^{1/2}$. Using the previously derived linear relation between λ and A, we also find $A \sim j_E' t^{1/2}$.

When $-1/4 < j_E' < 0$, from Eq. (10), the steady states should be stable for all q_1 when

$$\langle \phi_0^2 \rangle > \frac{1}{3}[1 - 2(-j_E')^{1/2}]. \tag{11}$$

This criterion indicates that the upper part of the branch between the green stars in Figs. 3(a) and 3(b) should be stable, while the lower parts close to λ_+ should be unstable [32]. This is similar to the Eckhaus instability criterion. Such a result suggests that the system is stuck once the dynamics hits the stable part of the steady-state branch, and as a consequence, it cannot evolve toward the minimum of $\mathcal{L}$ at $\lambda = \lambda_{\mathcal{L}}$.

Full dynamics.—These results are confirmed by the full numerical solution of Eq. (4) starting from small random perturbations of a flat state in a system of size $L = 500$. The results are shown in Fig. 4. First, and as expected, we find stable dynamics for $j_E' < -1/4$.

For destabilizing electromigration $j_E' > 0$, perpetual coarsening is found, as shown on Fig. 4(a), and after a transient related to the linear instability, the dynamics follows the steady-state branch in the (λ, A) plane, as shown in Fig. 2(a). We also confirm the scaling laws given above in Fig. 2(b) and find the prefactors: $\lambda \approx 1.4(j_E')^{1/2} t^{1/2}$ and $A \approx 0.22 j_E' t^{1/2}$. The ratio of these prefactors is in perfect agreement with the asymptotic behavior of the steady states discussed above $A \approx 0.16(j_E')^{1/2} \lambda$.

For weakly stabilizing electromigration $-1/4 < j_E' < 0$, the dynamics starts with a rapid increase of the amplitude at the most unstable wavelength of the linear instability, as shown in Fig. 3(a). Then, the average wavelength increases before the dynamics hits the steady-state branch at $\lambda = \lambda^*$,
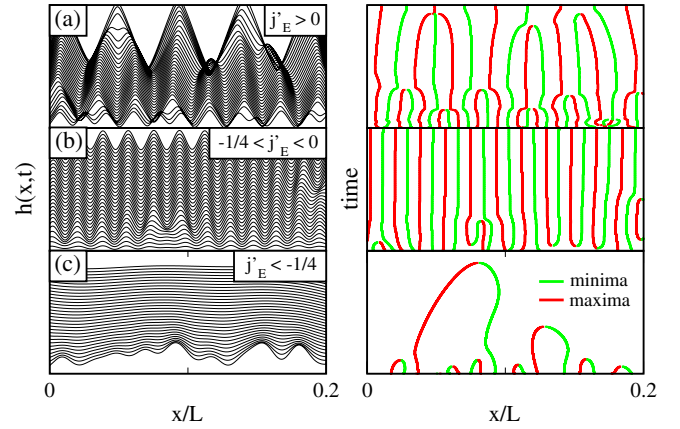

FIG. 4 (color online).   *Full dynamics and coarsening*—Left: Surface height $h(x, t)$ as a function of space for different times in the three different regimes: (a) $j_E' = 0.45$, (b) $j_E' = -0.15$, (c) $j_E' = -0.3$. Right: Corresponding spatiotemporal portrait of the extrema of the height profile.

as shown in Fig. 3(a). When the dynamics reaches the steady-state branch, it stops, as expected from the above prediction of steady-state stability. As a consequence, the system never reaches the minimum of $\mathcal{L}$ along the steady-state branch.

In order to check further the stability of the steady-state branch, we have performed simulations in boxes of width around 80 periods starting with periodic steady states with small perturbations. These simulations confirm the stability of the upper part of the branch and the Eckhaus-like instability of the lower part, in quantitative agreement with the condition (11). As seen in Fig. 3(a), the instability does not lead to a trajectory of the system along the steady-state branch in the (λ, A) plane. Instead, the trajectory escapes from the branch and returns to it, stopping in the same region as the dynamics from flat initial conditions. Fig. 3(b) summarizes the evolution of the different lengthscales as a function of j_E'.

Conclusions and perspectives.—In summary, we have studied the control of the faceting instability by means of electromigration. When electromigration is destabilizing, perpetual coarsening is found with a coarsening exponent $1/2$. For strong stabilizing electromigration, the surface is stable. Under weakly stabilizing electromigration, the surface exhibits a periodic cellular structure with a nonlinearly selected wavelength.

In the literature, nonlinear wavelength selection in mound growth [16], atomic step meandering [17], ion sputtering [33], and quantum dot formation in heteroepitaxial growth [34] has been interpreted as resulting from an instability of steady states, which stops at some point [18]. This scenario is usually referred to as interrupted coarsening [18]. However, the nonlinear wavelength selection scenario presented in this Letter does not correspond to interrupted coarsening, or to another instability of steady

states such as in the Eckhaus instability [19]. Indeed, we only observe coarsening *before* the dynamics hits the steady-state branch. Once the system reaches a steady state, it is stable and the evolution stops.

These results may provide hints to understand other nonlinear wavelength selection scenarios obtained in the literature, such as in the combination of growth and faceting as discussed in Refs. [29,30] (where nonlinear wavelength selection occurs between a coarsening regime, and a chaotic regime). More generally, we hope that our work will provide milestones toward novel methods to control the size of nanostructures emerging from surface morphological instabilities.

---

[1] A. Chame, S. Rousset, H. Bonzel, and J. Villain, Bulg. Chem. Commun. **29**, 398 (1996).

[2] Y. Kim, M. H. Jo, T. C. Kim, C. W. Yang, J. W. Kim, J. S. Hwang, D. Y. Noh, N. D. Kim, and J. W. Chung, Phys. Rev. Lett. **102**, 156103 (2009).

[3] H.-C. Jeong and J. D. Weeks, Phys. Rev. Lett. **75**, 4456 (1995).

[4] A. Di Carlo, M. Gurtin, and P. Podio-Guidugli, SIAM J. Appl. Math. **52**, 1111 (1992).

[5] F. Liu and H. Metiu, Phys. Rev. B **48**, 5808 (1993).

[6] L. Guillemot and K. Bobrov, Phys. Rev. B **83**, 075409 (2011).

[7] A. Latyshev, A. Aseev, A. Krasilnikov, and S. Stenin, Surf. Sci. **213**, 157 (1989).

[8] Y.-N. Yang, E. S. Fu, and E. D. Williams, Surf. Sci. **356**, 101 (1996).

[9] F. Leroy, P. Müller, J. J. Métois, and O. Pierre-Louis, Phys. Rev. B **76**, 045402 (2007).

[10] V. Usov, C. O'Coileain, and I. V. Shvets, Phys. Rev. B **83**, 155321 (2011).

[11] J. Krug and H. T. Dobbs, Phys. Rev. Lett. **73**, 1947 (1994).

[12] J. Chang, O. Pierre-Louis, and C. Misbah, Phys. Rev. Lett. **96**, 195901 (2006).

[13] C. Misbah, O. Pierre-Louis, and Y. Saito, Rev. Mod. Phys. **82**, 981 (2010).

[14] P. Kuhn, J. Krug, F. Hausser, and A. Voigt, Phys. Rev. Lett. **94**, 166105 (2005).

[15] V. Tomar, M. R. Gungor, and D. Maroudas, Phys. Rev. Lett. **100**, 036106 (2008).

[16] P. Politi and J. Villain, Phys. Rev. B **54**, 5114 (1996).

[17] G. Danker, O. Pierre-Louis, K. Kassner, and C. Misbah, Phys. Rev. E **68**, 020601 (2003).

[18] P. Politi and C. Misbah, Phys. Rev. Lett. **92**, 090601 (2004).

[19] W. Eckhaus, *Studies in Nonlinear Stability Theory* (Springer, Berlin, 1965).

[20] S. Stoyanov, Jpn. J. Appl. Phys. **30**, 1 (1991).

[21] O. Pierre-Louis, Phys. Rev. Lett. **96**, 135901 (2006).

[22] R. P. Johnson, Phys. Rev. **54**, 459 (1938).

[23] F. Haußer and A. Voigt, Phys. Rev. E **79**, 011115 (2009).

[24] J.-L. Lin, D. Y. Petrovykh, J. Viernow, F. K. Men, D. J. Seo, and F. J. Himpsel, J. Appl. Phys. **84**, 255 (1998).

[25] K. Sudoh, H. Iwasaki, and E. D. Williams, Surf. Sci. **452**, L287 (2000).

[26] H. Minoda, Y. Takahashi, Y. Tanishiro, and K. Yagi, Surf. Sci. **438**, 68 (1999).

[27] H. Minoda and K. Yagi, Phys. Rev. B **60**, 2715 (1999).

[28] D.-J. Liu and J. D. Weeks, Phys. Rev. B **57**, 14891 (1998).

[29] A. A. Golovin, A. A. Nepomnyashchy, S. H. Davis, and M. A. Zaks, Phys. Rev. Lett. **86**, 1550 (2001).

[30] T. V. Savina, A. A. Golovin, S. H. Davis, A. A. Nepomnyashchy, and P. W. Voorhees, Phys. Rev. E **67**, 021606 (2003).

[31] We use a finite difference explicit scheme.

[32] Because of numerical difficulties in the calculation of the steady-state branch for λ close to λ_+ when $0 > j'_E \gtrsim -0.1$, the upper steady-state stability limit (green stars) in Fig. 3(b) was obtained from an interpolation for $j'_E = -0.1, -0.05$.

[33] J. Muñoz-García, R. Gago, L. Vázquez, J. A. Sánchez-García, and R. Cuerno, Phys. Rev. Lett. **104**, 026101 (2010).

[34] J.-N. Aqua and T. Frisch, Phys. Rev. B **82**, 085322 (2010).